Growth of Large and Highly Ordered 2D Crystals of a K^+ Channel, Structural Role of Lipidic Environment

Rita De Zorzi,[†] William V. Nicholson,[†] Jean-Michel Guigner,[‡] Françoise Erne-Brand,[§] and Catherine Vénien-Bryan[†‡*]

[†]Laboratory of Molecular Biophysics, Department of Biochemistry, University of Oxford, Oxford, United Kingdom; [‡]Univ Paris 06, IMPMC, F-75252, Paris, France; and [§]Center for Cellular Imaging and Nano Analytics (C-CINA), Biozentrum, University of Basel, Basel, Switzerland

ABSTRACT 2D crystallography has proven to be an excellent technique to determine the 3D structure of membrane proteins. Compared to 3D crystallography, it has the advantage of visualizing the protein in an environment closer to the native one. However, producing good 2D crystals is still a challenge and little statistical knowledge can be gained from literature. Here, we present a thorough screening of 2D crystallization conditions for a prokaryotic inwardly rectifying potassium channel (>130 different conditions). Key parameters leading to very large and well-organized 2D crystals are discussed. In addition, the problem of formation of multilayers during the growth of 2D crystals is also addressed. An intermediate resolution projection map of KirBac3.1 at 6 Å is presented, which sheds (to our knowledge) new light on the structure of this channel in a lipid environment.

INTRODUCTION

To understand protein functions at a molecular level, high to intermediate resolution structures are an invaluable tool for soluble as well as for membrane proteins (1–3). Although many structures can be obtained by means of x-ray diffraction, electron crystallography has proven to yield high quality structures in the field of membrane proteins. The two techniques are similar in some aspects, but the information that they provide are complementary, because the conformation of the protein in 3D and 2D crystals is the result of different environments. In particular, the environment of the 2D crystals is more similar to the native environment of the protein and, thus, the structure determined by means of 2D crystallography is thought to be closer to the native one (4,5).

Obtaining good quality crystals, large enough to yield high-resolution information by imaging and diffraction, is a bottleneck in the structural determination by electron microscopy (EM) on 2D crystals. Whereas 3D crystallization robots are very popular and widely used, automatic systems available to perform 2D crystallization trials are much rarer. Usually, a large number of parameters have to be tested to find conditions in which the protein forms 2D ordered arrays and to optimize them (6). Although some theoretical studies about the effect of different parameters on 2D crystallization have been performed (7–9), a thorough and systematic experimental investigation is still the best way to achieve the crystal quality required for high-resolution studies. A number of papers reviewing the 2D crystallization conditions appeared in the last year and they provide useful information about parameters to be tested and their effect on the crystal growth (6,9–11). However, currently the amount of 2D crystallization data is still too low to provide a good statistical overview of this process.

In this work we revisited every step leading to membrane protein 2D crystallization, from protein expression to the production and growth of large and well-organized 2D crystals. In addition image analysis is covered. We present some valuable information and interesting conclusions applicable to other membrane proteins. Among the parameters investigated are protein purification, detergents, a large variety of lipids, and range of lipid to protein ratios (LPR), additives, the effects of temperature, and speed of detergent removal. We have tested four different methods of crystallization: dialysis, dilution, addition of BioBeads, or cyclodextrin. We have also addressed the problem of stacking of 2D crystals, which is often encountered during the formation of 2D crystals (12,13).

This work was done on a bacterial inwardly rectifying potassium ion channel, KirBac3.1. The inwardly rectifying potassium (Kir) channels comprise a super family of K^+ channels that regulate membrane electrical excitability and K^+ transport in many cell types (14). Kir channels are found in almost every cell in the body and control such diverse processes as heart rate, vascular tone, insulin secretion, and salt/fluid balance (15). Of the 80 different K^+ channel genes identified in the human genome, 15 belong to the Kir channel subfamily (Kir1.0–Kir7.0). Their physiological importance is further highlighted by the fact that genetically inherited defects in Kir channels are responsible for a number of human diseases (channelopathies) (15). Like all other K^+ channels, Kir channels are dynamic structures, existing in tightly regulated equilibrium between structurally distinct open and closed states. A number of x-ray crystallographic

Submitted August 2, 2012, and accepted for publication May 29, 2013.

*Correspondence: catherine.venien@impmc.upmc.fr

Editor: Andreas Engel.

0006-3495/13/07/0398/11

http://dx.doi.org/10.1016/j.bpj.2013.05.054

structures of KirBac1.1 and KirBac3.1 in a closed or nearly closed state have been published (16,17), as well as for the chimeric Kir/KirBac channel (18). The recent structure of GIRK2 (19) is not conductive. Very recently, we have solved the structure of KirBac3.1 in an open state where clearly, for the first time, the helix-bundle crossing is open (20). The open state was stabilized using the mutant S129R. However, our previous studies in cryo-EM (9 Å) (21), atomic force microscopy (22), and radiolysis foot printing (23) along with modeling for the gating mechanism (24), support the hypothesis that the channel, when in a native environment such as a lipidic bilayer, undergoes larger conformational changes upon gating than those proposed in our x-ray study. The environment of the ion channel is different in 2D (lipidic) than in a 3D (detergent) geometry. In addition, some constraints exist in the latter geometry compared to the former one, which could explain why the structure in 3D crystal might be less extended than in a lipidic environment.

In our previous work, projection maps from 2D crystals of KirBac3.1 wild-type (WT) were calculated in both the closed and open conformations (21). However, the calculation of the 3D structure of the open state by cryo-EM was limited at 9 Å resolution, hampered by a large variation of the unit cell parameters in the 2D crystals. The open state is not stable causing some change of conformation between 2D crystals making the 3D calculation impossible by the usual electron crystallographic approach. Through random mutagenesis and genetic complementation in K^+-auxotrophic *Escherichia coli* (*E. Coli*) and *Saccharomyces cerevisiae* (25), mutants that stabilize the open state have been identified.

In this work, we explain why the best results were obtained with a particular mutant of KirBac3.1 (S129R), and how we took benefit of the formation of the stacks of 2D crystals to grow very large and well-organized 2D arrays. Another crucial point such as the preparation of lipids added to the solubilized proteins before crystallization is addressed. All these conditions proved to be crucial for the growth of 2D crystals and the achievement of the high-resolution structural determination by electron crystallography. Furthermore, in the image analysis process, we have used an extra step of unbending, synthetic unbending, which has proved to be most important for the quality of the final map. We believe that these data provide valuable information applicable to other membrane proteins. Moreover, we have calculated an intermediate resolution projection map of KirBac3.1 at 6 Å, which sheds new light on the structure of this channel in a lipid environment.

MATERIAL AND METHODS

Protein expression and purification

The WT and two different mutants of the protein, S129R and S129R/S205R, were expressed and purified. The protein sequences have a 6-residue His-tag at the C-terminal end. A further construct was prepared by the insertion of a thrombin cleavage site before the His-tag in the S129R mutant in place of the last two residues (alanine and glutamine) of the protein sequence (S129R/Thrombin). This insertion allows the removal of the His-tag from the protein. The same expression and purification protocol was applied for the four proteins, see the Supporting Material.

Ternary mixtures: protein/detergent solutions mixed with lipid solutions

Straight after the gel filtration purification, the protein was mixed with lipids. Lipids were solubilized in detergent or resuspended in pure water and sonicated before use, see the Supporting Material for details. The latter is often used for reconstitution of proteins in liposomes. We are reporting for the first time that this method yields 2D crystals of high quality.

For each set of crystallization conditions, different LPR were tried. Initially, we tested a wide range of LPRs, from 0.2 to 1.0 w/w, whereas in the optimization process only a few LPRs were tested, around the optimal value observed in the previous step. After mixing of the protein in detergent solution with the lipids and eventually with additives, 0.02% of azide was added and the solutions were incubated overnight at 4°C. When *E. Coli* lipids were used without detergent, the solution remained cloudy even after mixing with the protein/detergent solution. In some crystallization trials 5 mM EDTA was added to stabilize the open state of the channel.

Crystallization trials

Dialysis experiments

The ternary mixtures (protein/detergent/lipid) were dispensed in Hampton Research (Aliso Viejo, CA) dialysis buttons, 50 to 100 μL sample volume, protein concentration 0.9–1.2 mg/mL, closed with a 10 kDa dialysis membrane. 3–4 dialysis buttons were then introduced into 50 mL Falcon tubes filled with a dialysis buffer. The buffer was changed every 24 h. After the first 4 days of dialysis, BioBeads SM-2 (Bio-Rad) were added to the buffer.

BioBeads experiments

30–60 μL of protein/detergent/lipid solution (protein concentration between 0.9 and 1.2 mg/mL) was introduced into microcentrifuge tubes and a single BioBead was added. The tubes containing the solutions were gently shaken on a rotator. Biobeads were added daily until no detergent was left in the sample, taking ~1 week and from 7 to 10 Biobeads. Usually, the last day of crystallization more BioBeads were added to eliminate the possible residual detergent. At the end of crystallization, the crystal solution was thoroughly mixed with a pipette and transferred into clean microcentrifuge tube to remove the BioBeads from the solution.

Dilution experiments

20 μL of protein-detergent-lipid solution (protein concentration: 2.6 mg/mL) was diluted with a detergent-free buffer (20 μL per addition), using different addition rates. A final volume of 400 μL, with a detergent concentration below the critical micelle concentration (CMC), was reached after 19 additions within 4 h, 3 days, or 7 days, at room temperature (RT). In all the trials, a white precipitate was visible and could be concentrated by centrifugation, before grid preparation.

Cyclodextrin (CD) addition

For these experiments, an automated system, the 2DX robot of the C-CINA research laboratory of the Biozentrum in Basel, was used with 96-well microplates (26). The experiments were designed to reach a concentration of detergent lower than the CMC at the end of the CD addition. To measure the exact amount of detergent in the protein solution the drop box method was applied (27). Through a titration with the CD solution,

methyl-β-cyclodextrin 5%, the exact amount to remove the detergent was evaluated. A volume of 35 μL of ternary mixture (protein concentration: 1.0–1.1 mg/mL) was dispensed in each well.

Different conditions have been tested thanks to the small amount required for each trial (50 μL).

Thrombin cleavage of the His-tag

Samples containing large multilayered crystals of the S129R/Thrombin were resuspended using a Hamilton syringe and incubated with ~1.5 units/mg of thrombin at RT for 7 days. Crystals in solution were resuspended twice daily over the incubation period using a Hamilton syringe to mechanically separate adjacent monolayers in stacked crystals by the exertion of shear forces. This procedure helps the enzymatic cleavage that would be otherwise hampered by the lack of accessibility of the cleavage site in the stacked crystals. His-tag removal was analyzed by sodium dodecyl sulfate-polyacrylamide gel electrophoresis (SDS-PAGE) and western blot analysis.

Transfer on electron microscope grids, image capture, and image analysis

For negative stain observations, crystal suspensions were examined in 2% uranyl acetate. We noticed that the crystals were sparse on hydrophilic grids. Therefore, we systematically used the carbon floated method, (see the Supporting Material). Negative staining is mainly used to increase the contrast of the sample and also to allow the fast screening of the crystallization conditions (28). Unstained specimens were prepared for high-resolution microscopy using the back injection method (28). Best results were obtained when sucrose 5–10% was present in the crystallization buffer (see the Supporting Material). Grids were frozen in liquid nitrogen. Images were collected using a CM120 (FEI-Philips Eindhoven, NL) equipped with a LaB6 filament, and a JEOL 2010F FEG (Tokyo, Japan) Micrographs were scanned on a Nikon Coolscan 9000. Alternatively, a Gatan CCD camera was used (4 k $\times$ 4 k).

Image processing was performed using the MRC suite of programs (29). The phases were corrected for the effect of the CTF as calculated by determining the position of the first zero of the CTF (CTFFIND2). The crystals were tetragonal $p42_12$. The phase origins of the set of 18 selected best crystals were refined at successively higher resolution out to 4 Å by minimizing the average phase residual (ORIGTILTK). Defocus and astigmatism were refined for each image by comparison with the averaged phases from all the other images by using the program CTFSEARCH. We used an additional step of unbending (synthetic unbending), which notably improved the quality of the final map. In this supplementary unbending, the merged projection of the best single images is used as reference and each crystal is unbent against this reference.

The image amplitudes were scaled as a function of resolution to compensate for resolution-dependent attenuation by using the program SCALIMAM3D with bacteriorhodopsin as a reference. The phases were constrained to either 0° or 180° because the projection is centrosymmetric in this plane group. Amplitudes and phases from the images were averaged as described previously (21). For some of the steps, we used the 2dx software (30,31).

Cross correlation (CC)

Following the protocol described in (21), the 3D model of KirBac3.1 S129R (3ZRS) (20) and the open 3D model (21,24) were filtered to 6 Å, projected onto the plane of the membrane and rotated in the plane. Each projection was cross-correlated with the cryo-projection map, and for each model the rotation values giving the best CC result were chosen. For details, see (21).

RESULTS AND DISCUSSION

We have tested >130 different parameters. All the conditions are described in Table S1. A meaningful summary for this exhaustive research is shown in Table 1.

Reproducibility

For every trial included in the work, a control was added in the same conditions known to yield crystals to check the quality of the starting protein. For each trial, more than one LPR was tested, typically four or even more, and the trend was observed. Trials with low reproducibility were easily recognized and ruled out.

Protein purification, stability in detergent

From the experience with KirBac3.1, we observe the purification of the protein to be a key step in the preparation of good quality 2D protein crystals. Noticeable differences were observed in different preparations. An important observation is that protein solubilized in detergent, tridecyl-β-D-maltoside (TDM) 0.5 mM, tends to aggregate at RT, even at concentrations lower than 3 mg/mL. Thus, the setup of the crystallization experiments straight after the gel filtration has to be preferred, because aggregation and precipitation were observed even after an overnight incubation at 4°C in solutions with protein concentrations >10 mg/mL. An amount of 5% (w/w) of lipids in a similar solution prevents the precipitation. A factor influencing the poor stability of KirBac3.1 is the presence in the solution of high concentrations of imidazole. A fast removal of imidazole after elution of the protein by buffer exchange was necessary.

Membrane preparation did not improve the protein quality for KirBac3.1, unlike that described for other membrane proteins (11).

One of the most important parameters to be taken into account in the choice of the detergent to use in solubilizing a membrane protein is its CMC. If a dialysis protocol is applied for the crystallization, the CMC of the detergent influences also the rate of detergent removal and, thus, the kinetic parameters of protein crystallization: low CMC requires longer times of dialysis and slows down the rate of detergent removal, whereas detergents with high CMC values are faster removed from the protein/lipid solution. Equally important is the stability of the protein in a solution of the detergent at a concentration sufficient to prevent protein aggregation (32) and keeping the protein in a native conformation. The use of BioBeads for detergent removal overcomes problems arising from protein stability in detergent, because the detergent removal rate in these experiments is very fast and not influenced by its CMC (32).

To solubilize KirBac3.1, two different detergents have been tested. The first choice was TDM, in which the WT

TABLE 1 Summary of the crystallization results in different conditions with asterisks marking the quality of the crystals obtained

[a]	Method[b]	Lipids	LPR	Detergent	Detergent removal	Additives	T	Results
WT	Dialysis	PIP2/DOPC (from 50:50 to 5:95) in DHPC	0.7–1.0	TriDM/DHPC	Slow	–	RT	Small crystals
SM DM	Dialysis BioBeads CD[b]	DOPC, DOPC in DHPC, DOPC in DM	0.4–1.0	TriDM, TriDM/DM, TriDM/DHPC	Slow and medium	With or without 5% sucrose	RT, 37°C[c]	Aggregates and small crystals at LPR = 0.8–1.0 at border of aggregates, best results at 37°C with CD
SM DM	Dialysis BioBeads CD[b]	DMPC, DMPC in DM, DMPC in DHPC	0.2–1.0	TriDM, TriDM/DM, TriDM/DHPC	Slow and medium	With or without 5% sucrose	RT, 37°C[c]	Aggregates and empty vesicles, arrays seen only in a few conditions, best results at 37°C with CD
SM	CD[b]	PS/PE/PC	0.2–1.0	TriDM	Medium	–	RT	Aggregates and empty vesicles
SM	Dilution	Polar	0.6–0.9	TriDM	Fast to slow	–	RT	Large crystals, multilayers*
SM DM	CD[b]	Total or Polar	0.6–0.9	TriDM	Slow and very slow	0–5% sucrose, 0–10 mM $MgCl_2$	RT, 37°C[c]	Crystals, very big***, better results with 5% sucrose at LPR = 0.7–0.8
WT DM	Dialysis BioBeads	Total, Polar, total in DHPC or Polar in DHPC	0.7–0.8	TriDM	Slow	0–5 mM EDTA, 0–5% sucrose	RT	Tubes and crystals, smaller with WT
SM	Dialysis	Total in DM	0.6-1.0	TriDM/DM	Slow	–	RT	Aggregates and some organization at LPR = 0.8–1.0
SM	Dialysis BioBeads	Total or Polar	0.7–0.9	TriDM	Slow	2.5 mM EDTA, 0–5% sucrose	RT	Large crystals**
SM	Dialysis BioBeads dialysis and sonication	Total or Polar (sonicated or not)	0.7–0.8	TriDM	Slow	5 mM EDTA, 5–10% sucrose, 0–0.3M KCl (last dialysis buffer, after 6 days)	RT	Large crystals, some are monolayers***, better with dialysis, adding 5 mM EDTA and 10% sucrose
SM	Dialysis BioBeads	Total or Polar	0.4–1.0	Hega-10	Slow	2.5 mM EDTA	RT	Aggregates and empty vesicles
WT SM DM	Dialysis	Total or Polar	0.7–0.8	TriDM	Slow	(5 mM EDTA, 5–10% glycerol) or 0.5 mM $CoCl_2$ or 300 mM KCl or 50 mM–0.1M $MgCl_2$	RT	Aggregates and empty vesicles
SM	Dialysis	Total or Polar in TriDM	0.7–0.8	TriDM	Slow	5 mM EDTA	RT	Aggregates and empty vesicles

[a]SM = KirBac3.1 S129R; DM = KirBac3.1 S129R/S205L; WT = KirBac3.1 Wild-Type.
[b]CD = cyclodextrin method.
[c]37°C = incubation at 37°C for 1–2 h during crystallization.

is stable. Although the time required to remove the TDM from the ternary mixture is longer than a week due to the low CMC (0.033 mM in water, 0.024 mM in NaCl 150 mM, Anatrace measurement), no aggregation was observed providing that the amount of lipids added was sufficient. Decanoyl-N-hydroxyethylgucamide (Hega-10) was tested in dialysis and BioBeads experiments. Hega-10 was chosen because it was crucial for the growth of 3D crystals (20). Unfortunately, the dialysis trials were unsuccessful. The reason is unclear, but we hypothesis that the fast removal rate of Hega-10 plays a role. Indeed, Hega-10 has a CMC of 7 mM in water. Thus, we expect the detergent removal to be >100 times faster for Hega-10. In addition, no 2D crystallization using Hega-10 has been reported so far. As for the BioBeads experiments with Hega-10, some crystal formation was observed, although no large sheets could be obtained, indicating that aggregation is faster with this detergent than with TDM and occurs before crystallization.

Lipids: nature and concentration

The choice of the lipids that form the lipid bilayer is pivotal to help favorable protein-protein and protein-lipid interactions that lead to the crystal formation. In addition to dioleoyl phosphatidilcholine (DOPC) solubilized in diheptanoyl phosphatidilcholine (DHPC), used in a previous work (21), we tested also dimyristoyl phosphatidylcholine (DMPC), 1-palmitoyl-2-oleoylphosphatidylcholine (POPC), *E. Coli* polar and total lipid extracts, different ratios of phosphatidylserine/phosphatidylethanolamine/phosphatidylcholine (PS/PE/PC), and phosphatidylinositol

4,5-bisphosphate (PIP_2)/DOPC mixtures. DMPC, in particular, was chosen because it has been reported to be one of the most successful lipids for 2D crystallizations (33), whereas *E. Coli* lipids have proven to be useful in the case of aquaporins (1,34). With the mixture PS/PE/PC, no crystals could be grown. Results obtained with DMPC were not reproducible. Polar and total *E. Coli* lipid extracts yielded tight arrays and larger sheets than those obtained with DOPC. 2D crystals were also observed with the PIP_2/DOPC mixtures, ratio from 5:95 to 25:75 (w/w).

We noticed that the lipid nature is a key parameter to obtain good quality crystals. In particular, the experiments were very reproducible only when *E. Coli* lipid extracts or DOPC were used, whereas no crystallization at all was observed in the other trials (Fig. 1, *A–C*), even when changing parameters, such as additives, rate of detergent removal, or temperature. The nature of lipids influences the quality of 2D crystals; indeed, when DOPC was used, the crystalline arrays were quite loose (whatever LPR ratio successfully used to produce 2D crystals, see Table 1 and Table S1) (Fig. 1 *D*), whereas the lattices observed with *E. Coli* lipids looked very ordered and clearly visible from the negative staining (NS) samples, recognizable also in cryo conditions (Fig. 1, *E* and *F*). It is important to note that the best crystals obtained with *E. Coli* lipids had a LPR of 0.7, whereas the best obtained with DOPC lipids were grown from LPR 0.7. LPR of 0.7 with DOPC produced only a few and not well-ordered crystalline arrays together with protein aggregates. Experiments with different lipids have been treated independently: a first screen was performed at various LPRs (typically between 0.2 and 1.2, steps of 0.2). In the case of positive hits, a smaller range and smaller step were used to refine the crystallization conditions.

As the detergent affects the protein stability, it should be chosen carefully. For KirBac3.1 different detergents have been used to solubilize the lipids before the preparation of ternary mixtures: TDM, which is known to stabilize the protein as it has been used throughout all the purification; decyl-β-D-maltoside (DM), also used for the initial solubilization step and with a higher CMC than TDM and, thus, removed more quickly; DHPC, used successfully with DOPC (21).

Most importantly, some trials with *E. Coli* lipids have been carried out without addition of detergent to the lipid solution. The suspension obtained was sonicated before mixing with the protein solution for 3 h, but was still milky. Even upon addition of sonicated lipids to the protein-detergent solution, the milky aspect was still present. The use of the solution of lipids in pure water or solubilized in TDM was conducive to 2D crystallization in both cases. In the former case, however, the dimensions of the crystals were larger, probably due to the lower amount of detergent in the starting solution. The present result shows that the very small liposomes made during the sonication step in pure water are not completely solubilized when added to the mixed protein/detergent solution. However, the lipid bilayers of the liposomes are most probably destabilized by the detergent, allowing the insertion of the protein into the lipid bilayer (35). We consider that this slight variation in the traditional protocol was surprisingly successful and we would recommend trying it with any other membrane protein.

After selection of the most suitable lipids for 2D crystallization, the correct LPR has to be identified (Fig. 2). However, we chose to setup always more than a single LPR experiment, because the concentration of the copurified lipids may modify the actual LPR and, although in all the experiments the same protocol was applied, even small variations of the LPR are reported to affect the results (33).

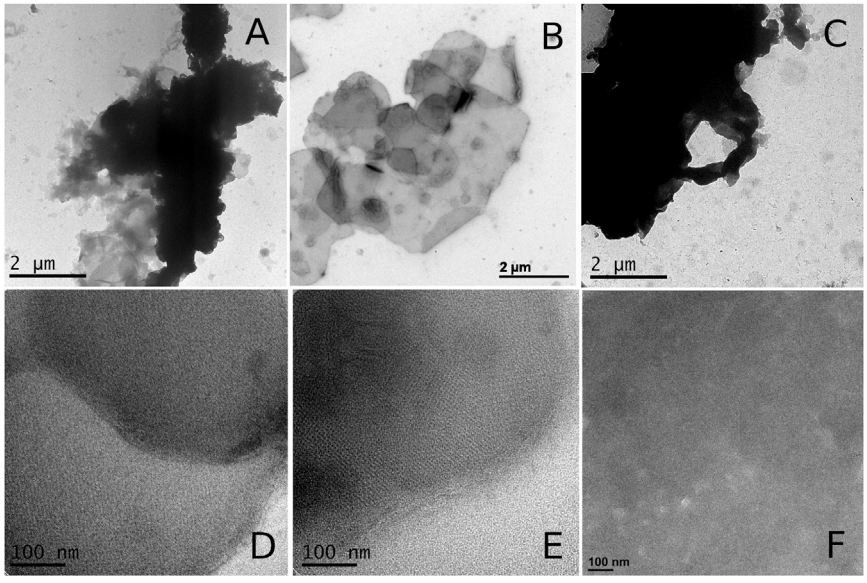

FIGURE 1 Crystallization in the presence of different lipids: (*A* and *D*, NS-EM) in DOPC (LPR = 0.70, crystallized by BioBeads addition) large aggregates are formed, however, at the border of these, small ordered arrays are recognizable; (*B* and *E*, NS-EM) the use of *E. Coli* Lipid Extracts (LPR = 0.75, BioBeads addition) yields crystal sheets; (*C*, NS-EM) DMPC (LPR = 0.80, dialysis) yields only empty liposomes and protein aggregates; (*F*, cryo-EM) Crystal of S129R/Thrombin obtained with *E. Coli* total lipid extract (LPR = 0.70, dialysis in the presence of sucrose 10%), after thrombin cleavage of the His-tag.

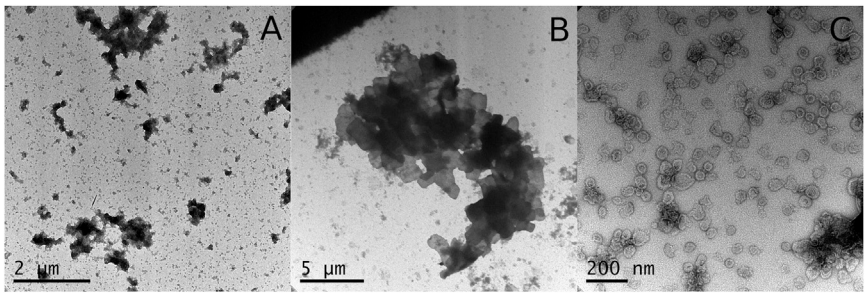

FIGURE 2 Effect of the lipid protein ratio on crystallization: (*A*) protein aggregates are formed for low LPR (0.4); (*B*) the correct LPR (0.7) yields crystal sheets with square borders; (*C*) in case the amount of lipids is too high in comparison with the protein (LPR = 1.0), proteoliposomes and empty liposomes are obtained, but no ordered arrays.

Crystallization method

For crystal formation, a key parameter turned out to be the overnight incubation of the ternary mixtures. When this step was omitted, no crystallization but rather protein aggregation could be detected. These observations seem to support again the idea that the crystal formation starts when the detergent is still present in solution. A further indication of the importance of the initial incubation of the protein in detergent with the lipids, even at high detergent concentrations, is the appearance of the solutions. A cotton-like soft precipitate was observed for all successful crystallization trials in the initial ternary mixtures.

Together with the CMC of the detergent, the method used for the crystallization affects the rate of detergent removal and, thus, the formation of crystals. For this work we tested different crystallization methods (see Methods section) to compare their efficiency in yielding good quality crystals.

To assess which mechanism is involved in the crystal formation for KirBac3.1, we combined together the results of the different crystallization techniques. Samples were taken at different stages of detergent removal. In the dialysis and BioBeads experiments, centrifuging the crystal suspension and then exchanging the buffer with a detergent-free buffer allowed preparing NS grids at different stages of the crystallization experiments.

The dilution method is ideal to test different rates for the crystallization, as far as a high protein concentration (2.5–3 mg/mL) is available without aggregation. The results show that the crystal formation is a quick process after the first reduction in detergent concentration (32), although the quality is strongly influenced by the rate of detergent removal. Small crystal sheets could be observed even when the dilution was performed in 3 h. Formation of crystals was observed even in the presence of residual detergent. Our hypothesis is that the formation of stacks and, more generally, the presence of the His-tag (see below) help to promote insertion of the protein into lipid bilayers and/or formation of 2D crystals even before the detergent is completely removed.

From the results of this systematic study, we came to the conclusion that protein-detergent interactions are weaker than those between protein and lipids (36). This accounts also for the stabilization of the protein observed upon lipid addition, whereas aggregation and precipitation is fast if only detergent is present.

Moreover, when crystals are obtained using lipids without detergent, we hypothesize that 2D crystallization of KirBac happens with a three-stage mechanism as described previously (9,32). In the case sonicated lipids without detergent are used, the bilayer is already present in suspension (32,35). In this case, the second step consists in the insertion of the protein in the preformed bilayer destabilized by the presence of detergent in the protein solution, whereas the third is the proper crystallization. A slightly different mechanism is expected for crystals obtained from detergent-solubilized lipids.

The use of the 2DX robot of the C-CINA research laboratory of the Biozentrum in Basel (26), is invaluable as it enables to test many 2D crystallization conditions such as lipid, detergent, additives, rate of detergent removal. The dilution method allows having a quick idea of the feasibility of crystallization but is only possible if enough protein is available. The best crystals were obtained with the dialysis and the BioBeads methods.

Other parameters affecting crystal quality

As for 3D crystals, the temperature at which the crystallization process is carried on influences the energetic parameters of the process. For instance, the increase of temperature is suggested for lipids with a phase transition above the RT, such as DMPC (9). However, for Kirbac3.1, no difference was observed between the RT experiments and those in which 1-h cycles at 37°C were carried out every day during the crystallization process. In particular, in the case DMPC (transition temperature: 23°C) was used, results suggest that lipid fluidity does not improve the crystallization that is more sensitive to membrane formation and, thus, depends on the lipid nature more than on the phase transition temperature. A similar behavior was reported for crystals of human leukotriene C_4 synthase (33).

Additions of salts and sugars to the crystallization solution have also been tested. We noticed that the increase of the ionic strength of the solution by increasing the salt concentration hampers the formation of crystals, whereas sucrose and glycerol seem to have a positive effect in

crystallization. Moreover, sucrose was found to help prevent the stacking formation, although not removing completely interactions between sheets.

Another parameter to be taken into account is the volume of the crystallization solution, because scaling up is often associated with slight variations in the optimal conditions. In the case of KirBac3.1, doubling the total amount of solution used, from 50 to 100 μL for the dialysis experiments and from 30 to 60 μL for the crystallization in presence of BioBeads, yields the same quality of crystals.

Formation of stacks of 2D crystals

The formation of stacks of 2D crystals was noticed in all the crystallization conditions tested in this work, although the extent of the stacking differed according to various parameters. However, the presence of more than one layer in the crystalline sheets was hard to determine by NS-EM on non-tilted specimen.

As previously reported (33), we noticed an increase in the degree of stacking formation by ageing. When samples kept at 4°C were analyzed after a month, more multilayers (up to 10) were observed in comparison with the fresh samples, for which grids were prepared just after the end of crystallization.

Different strategies have been applied to try to disrupt the stacks and obtain single layers on the grids. A possible way to achieve this result is to apply a mechanical stress on the stacked crystals: if the interlayer interactions are weaker than the intralayer, the disruption of the stacks should happen before the disruption of the crystal lattice. To this purpose cycles of flash freezing and quick thawing, carried out just before grid preparation, and sonication of the crystals in a water bath for different periods, up to 2 min, revealed to be ineffective. In particular, in the latter case we could observe a loss of crystallinity in the sheets before the stacks were sensibly disrupted. A better result was obtained by suction and reinjection of the crystal suspension through the metallic needle of a Hamilton syringe ~20 times. In this case the decrease in the amount of stacks observed on the grid was significant but they were still mainly present.

A different strategy consisted in the addition to the crystallization buffer of chemicals that could prevent or disrupt the interactions between layers. A first trial was carried out at higher salt concentration (KCl 300 mM), with the aim to create competitive interactions between the salt ions and the protein hydrophilic domains protruding from the membrane. Unfortunately, the increase in the salt concentration greatly hampered the formation of the crystals or resulted in a loss of crystallinity after they were formed. When 20% sucrose was added to the crystallization buffer, fewer multilayers were observed on the NS grids. The large percentage of sucrose that was used, however, made the preparation of cryo-grids very difficult due to the viscosity of the solution. An attempt to reduce the concentration of sucrose in the buffer after crystallization did not improve the result, because the number of crystal stacks was increased.

Results from all the crystallization experiments are summarized in Table 1 (full list of the crystallization experiments in Table S1).

In some crystallization experiments, together with the stacked crystals, we noticed the presence of tubular structures (Fig. S1). These tubes showed weak diffraction. Our conclusion is that these tubes are not helical crystals, but simply sheets rolled up, as previously reported for purple membrane crystals (9,37) and for H^+-ATPase crystals (32). Probably the same interactions responsible for the stack formation are involved in the tendency of these crystals to form rolls.

Despite some degree of success, none of the previous approaches was able to yield a sufficient amount of monolayers needed for the 3D reconstruction from EM images of tilted specimens. The degree of stacking formation for this particular protein is too severe and prevents the image analysis.

Interactions leading to the formation of stacks

The formation of stacks of 2D crystals was first indicated by subtle changes of the darkness of the stain on what appeared as a single sheet upon observation of negatively stained 2D crystals using EM. A more careful analysis of the borders of the sheets confirmed the presence of more layers, although almost perfectly overlapping. From this observation, we hypothesized the presence of a specific interaction that drove the formation of multilayers, because in most of the cases crystals of KirBac3.1 forming stacks are in register.

Although some details indicate the presence of more than one layer of crystal, on NS untilted grids recognizing the presence of stacks and evaluating their number and their thickness was not trivial (Fig. 1 *B*, Fig. 2 *B*, and Fig. 3 *A*). However, on images taken from samples tilted at high tilt angles (between 40° and 60°), it was possible to count up to 10 layers of crystals, with a total thickness of ~0.1 μm (Fig. 3 *B*). Image analysis from 12 NS stacked crystals was done and results are shown in Fig. S2. The reason why the 2D crystals form stacks became clear when we solved the 3D structure of KirBac3.1 using x-ray crystallography (24). The analysis of the packing of the 3D crystals shows that these 3D crystals appear to be piles of 2D sheets, although no membrane surrounding the protein could be detected (Fig. S3). The absence of lipid membrane in these crystals was verified using the analysis of low-resolution diffraction intensities (data not shown, R. De Zorzi). This method has been reported previously for membrane proteins forming crystals of the so-called type I, i.e., with pseudo-2D crystals orderly piled in the third dimension (38). Moreover, the arrangement of the proteins in the horizontal direction, i.e., the direction of the pseudo-2D sheet (Fig. S3 *A-B*), is

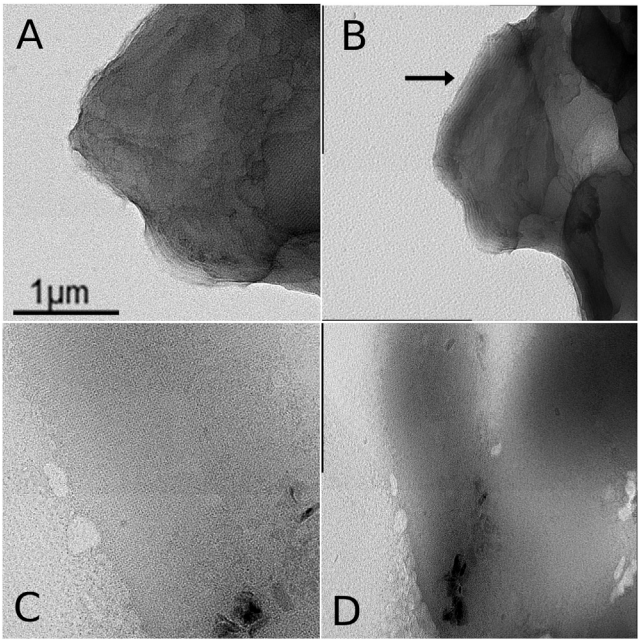

FIGURE 3 2D crystals multilayers and monolayer (*A*) NS-EM image of a stack of crystals at 0° tilt. (*B*) The same specimen at 60° tilt. About 10 layers are visible at the edge of the crystal (see *arrow*). (*C*) NS-EM image of a crystal of KirBac3.1 S129R/Thrombin, crystallized and cleaved using thrombin. The lattice pattern is still visible. (*D*) The same crystal at 40° tilt. No stacks can be detected.

very similar to that postulated for the 2D crystals according to the symmetry observed, $p22_12_1$. A closer observation of the interactions responsible for the packing in the 3D crystals revealed that the His-tag plays a key role. In addition, several hydrophilic interactions are in place between 2 amino acids just before the His-tag. A similar hypothesis about the formation of stacks of 2D crystals have been formulated for other proteins in which protruding structural domain were thought to be responsible for interactions between 2D layers of crystals (33). In this case, the possibility of a close analysis of the 3D structure gives further reliability to a similar hypothesis. Moreover, the phenomenon observed in the 2D crystallization trials, with the extent of stack formation increasing with ageing, may be directly referred to the mechanism of growth of the 3D crystals (9,13).

In the 3D structure from x-ray diffraction, four strong H-bonds between the backbones of three residues just before the His-tag (Ile-293, Ala-294, and Gln-295) held together protein that belong to adjacent pseudo-2D sheets, with the bond distances ranging between 2.8 and 3.0 Å (Fig. S3 *C*). Although the H-bonds involve the last residues of the protein sequence, the His-tag is thought to stabilize the formation of these bonds by weaker electrostatic interactions.

The previous observations suggest that a strategy to remove the stacking problem for 2D crystals is the disruption of the strong interactions observed in the 3D structure. Thus, we designed another construct, containing a thrombin cleavage site before the His-tag (S129R/Thrombin), allowing the removal of the mentioned interactions between 2D crystal sheets.

Cleavage of the His-tag removes the tendency to form stacks

First attempts to crystallize the S129R/Thrombin protein after cleavage of the His-tag by incubation with thrombin produced single-layered crystals but of poorer quality than these obtained with protein with His-tag. The formation of crystals was observed in the optimized conditions (defined with the other protein construct), but somehow smaller in size (0.3 μm). The conditions may need to be adjusted to obtain crystals of similar size as for the His-tagged protein.

An alternative strategy was the removal of the tag after crystallization. Crystals formed by the dialysis method in the presence of *E. Coli* total lipid extract were selected for thrombin cleavage due to their large size and high degree of order within the lattice as identified by NS-EM. Separation of the layers of such crystals yielded 2D crystals of a large enough size and good enough quality to be analyzed by electron crystallography.

Because the packing of the cytoplasmic domains in stacked crystals is expected to be very tight, mechanical disruption was necessary to allow access of thrombin to the cleavage sites, otherwise buried within the crystal stacks. Shear stress exerted on crystals by resuspension using a Hamilton syringe is sufficient to allow temporary disruption of crystal stacking to allow for a high level of thrombin cleavage, as visualized by western blot analysis (Fig. S4).

Experiments were carried out at RT and 30°C. The increase in temperature is expected to affect the hydrophilic interactions formed between stacks to a greater extent than it affects the hydrophobic interactions responsible for reconstitution and crystal packing in the bilayer, thus further promoting the separation of stacks (9). However, results from EM show no difference in stack separation in the tested temperatures.

Analysis of cleaved crystals by NS-EM showed that the overall dimensions and degree of crystallinity were unchanged with respect to the stacked crystals and many monolayer crystals could be clearly identified in the electron micrograph in addition to a small number of remaining multilayers (Fig. 3 *C* and Fig. S5). The number of layers of the cleaved crystals was checked by tilting the samples under the electron beam, as previously described, and the resulting images (Fig. 3, *C* and *D*) confirm the monolayer nature of these samples. It is difficult to quantify precisely the proportion of multilayers still present on the EM grid, however the His-tag still present after thrombin treatment has been calculated to be $<5\%$ (from the western blot gel, Fig. S4 *B*).

Moreover, image analysis was further performed on these monolayer 2D crystals and was conductive to a map at intermediate resolution, demonstrating that the order of the crystal lattice is not affected by thrombin cleavage.

The mutant (S129R) stabilizes the unit cell parameters

Growth of 2D crystals using the mutant Kirbac3.1 S129R proved to be crucial to obtain more constant cell parameters and structural information at high resolution:

A statistical analysis of unit cell parameters from the WT KirBac3.1 2D crystals shows high variability: $a = 98 \pm 4$ Å, $b = 107 \pm 5$ Å, $\gamma = 90 \pm 1^\circ$ with $p22_12_1$ symmetry (B. Zadek and C. Vénien-Bryan, personal data and Graph S1) making difficult or impossible the merging and calculation of the 3D structures from these 2D crystals. The mutant Kirbac3.1 S129R stabilizes one particular state of the protein (open conformation) preventing large variations of the unit cell: Unit cell parameters for 2D crystals of Kirbac3.1 S129R reconstituted in *E. Coli* lipids (stacked 2D crystals) were typically $a = 103 \pm 1$Å, $b = 110 \pm 1$Å, $\gamma = 90 \pm 1^\circ$ with $p22_12_1$ symmetry. Moreover, 2D crystals of the S129R/Thrombin, after thrombin cleavage (monolayer 2D crystals) have still a low variability of the unit cell dimensions due to the stabilizing mutation: $a = b = 108 \pm 1$Å, $\gamma = 90 \pm 1^\circ$ (Graph S2), however, they show a tetragonal symmetry $p42_12$. This slightly different symmetry might be due to the release of constraints, i.e., the packing in the third dimension.

2D crystals of KirBacS129R in cryoconditions

The computed diffraction pattern of KirBac3.1 S129R after thrombin cleavage gave a tetragonal unit cell with dimensions $a = b = 108 \pm 1$ Å. 47 crystals were chosen for further processing. The crystal area was corrected for lattice distortions, merged and averaged in $p42_12$. Raw phases were rounded to 0° or 180° and phase residuals were calculated from the absolute values of the rounding errors (Table 2). Fig. 4 *A* shows the cryoprojection map of 18 averaged and symmetrized crystals at 6 Å.

We found that the quality of the map improved dramatically when we further unbend each crystal using as a model a synthetic map previously made by merging all the images (Fig. 4 *B*). After this supplementary unbending step, the mean values for the figures of merit (as given by the software AVRGAMPHS (29)) for different resolution shells improved dramatically (Fig. 4 *B*). Projection maps from three single crystals used in the merging step are shown Fig. S6.

TABLE 2 Image analysis statistics

Plane group symmetry	$p42_12$
Unit cell dimensions	$a = b = 108$ Å, $\gamma = 90^\circ$
Total number of reflections	1413
Number of unique reflections	288 (up to 6 Å)

Resolution ranges	Phase residual (random = 45°)	Figure of merit
200–12.6	17.4	0.95410
12.6–8.9	24.8	0.99251
8.9–7.3	35.1	0.96899
7.3–6.3	30.2	0.96222
6.3–5.7	43.9	0.92780
5.7–5.2	88.3	0.85015
5.2–4.8	79.8	0.86395

Interpretation of the map

To interpret the density peak of the cryo-projection map, we performed a CC between known 3D structures either calculated from 3D crystals in detergent (3ZRS and 2WLH), or modeled from 2D crystals in lipid bilayer; and our 2D projection cryo-map, Fig. 5.

The CC value between the 2D cryoprojection map of KirBacS129R and the calculated structure of the same protein in 3D, crystallized in detergent, (3ZRS, bundle crossing in open conformation) was 0.58 (Fig. 5 *A*), similar to the CC value obtained comparing the closed conformation of the channel (2WLH) and our projection map (0.57), but much lower than the CC value between the 2D cryoprojection map and the predicted model of KirBac1.1 open state in lipid environment, 0.69 (Fig. 5) (21,24). This study supports our previous published work (20,21,24), the channel, when in a native environment such as lipidic bilayer, undergoes larger conformational changes upon gating than those proposed in our x-ray study. Noticeably, the outer helices seem to undergo larger movement toward the outside. Indeed, the angle the outer helices make to the normal of the membrane surface is 30° compared to the 10° in the structure 3ZRS.

CONCLUSIONS

Electron crystallography is a technique that has a great potential in the field of structural determination for membrane proteins. The major asset of this technique is that the protein is embedded in a lipid bilayer, its natural environment. However, 2D crystallization may be very difficult for some proteins and often requires a thorough screening.

In this work, we have defined the best experimental conditions to obtain 2D crystals of KirBac3.1 suitable for studies at high resolution. Following this systematic analysis, where >130 different parameters were tested, we can propose key parameters that are crucial to produce reproducibly large and very well-ordered 2D crystals suitable for image analysis at high resolution:

1) The use of a KirBac3.1 mutant was crucial to stabilize one particular state of the protein (open conformation) and prevents large variations of the unit cell parameters between 2D crystals that hamper the study at high resolution.
2) KirBac3.1 formed larger crystals when *E. coli* lipid solution was only sonicated (in water) but not solubilized in detergent.

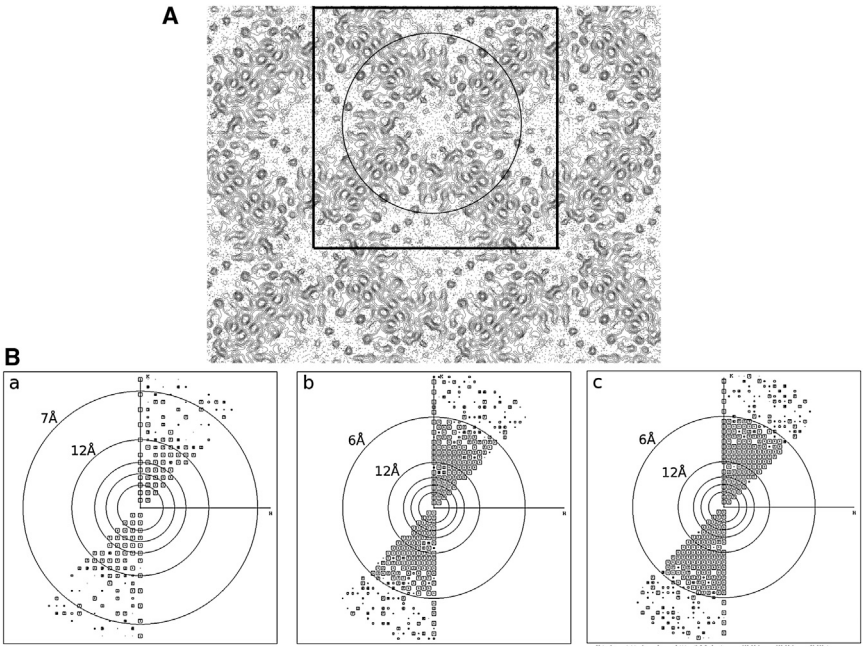

FIGURE 4 Image analysis from cryo-EM images of monolayer crystals (*A*) Projection map from images of untilted KirBac3.1S129R thrombin cleaved 2D crystals. One unit cell is outlined, $a = b = 108$ Å, $\gamma = 90°$ (*B*) Plots of the phase residual values for the merged reflections. Values correspond to phase residuals: $1 < 8°$, $2 < 14°$, $3 < 20°$, $4 < 30°$, $5 < 40°$, $6 < 50°$, $7 < 70°$, $8 < 90°$ (reflection whose statistics are below 4 are shown only with small size boxes). (*a*) Plot obtained after the first merging step, using the best 18 images, unbent against Fourier filtered references; (*b*) after a merging step on images unbent against the (*synthetic*) reference obtained from (*a*); (*c*) final plot, obtained after scaling of the amplitudes of (*b*) against a Bacteriorhodopsin dataset (*sharpening*).

3) We took benefit of the formation of stacked 2D crystals (problem that is often encountered in 2D crystallization) to produce large and well-ordered 2D crystals. We developed a method to separate the monolayers from the stacks of 2D.
4) During the image analysis, we performed an extra step of unbending using the synthetic unbending, which noticeably improved our data and provided a projection map at 6 Å.

All this information provides much insight into the 2D crystallization of KirBac3.1, however, these findings could also be applied to other membrane proteins.

In addition, in this work, we present a cryoprojection map at 6 Å. The interpretation of this map supports the idea that embedded in a lipidic environment the conformation of KirBac is more open than described in the structure from 3D crystallography. The future development of this work will be the calculation of the 3D structure of KirBac3.1 from a series of images of tilted specimens taken with a high-performance microscope.

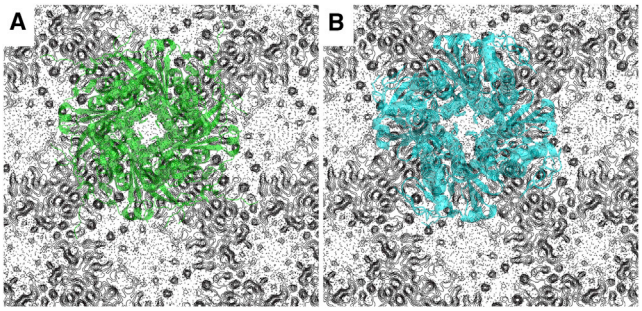

FIGURE 5 Fit of the crystal structures of KirBac on the 2D projection map: (*A*) Crystal structures of KirBac open state (PDB: 3ZRS, in *green*) on the 2D projection map. (*B*) Crystal structure of the open state model of KirBac1.1 (in *cyan*) (21,24) on the 2D projection map

SUPPORTING MATERIAL

Supporting analysis, methods, and reference (39) are available at http://www.biophysj.org/biophysj/supplemental/S0006-3495(13)00642-5.

We are grateful to Dr. Brittany Zadek for her early experiments and to Mr. Eric A. Bray for some experiments with thrombin cleavage.

This work was supported by grants from the Biotechnology and Biological Sciences Research Council (BBSRC) and the Wellcome Trust. R.D.Z. was supported by a Marie Curie Intra-European Fellowship. All authors declare that there is no conflict of interest.

REFERENCES

1. Hite, R. K., Z. Li, and T. Walz. 2010. Principles of membrane protein interactions with annular lipids deduced from aquaporin-0 2D crystals. *EMBO J.* 29:1652–1658.
2. Jonic, S., and C. Vénien-Bryan. 2009. Protein structure determination by electron cryo-microscopy. *Curr. Opin. Pharmacol.* 9:636–642.
3. Stahlberg, H., and T. Walz. 2008. Molecular electron microscopy: state of the art and current challenges. *ACS Chem. Biol.* 3:268–281.
4. Tsai, C. J., C. S. Ejsing, …, C. Ziegler. 2007. The role of lipids and salts in two-dimensional crystallization of the glycine-betaine transporter BetP from *Corynebacterium glutamicum*. *J. Struct. Biol.* 160: 275–286.
5. Tsai, C. J., and C. Ziegler. 2010. Coupling electron cryomicroscopy and X-ray crystallography to understand secondary active transport. *Curr. Opin. Struct. Biol.* 20:448–455.
6. Schmidt-Krey, I. 2007. Electron crystallography of membrane proteins: two-dimensional crystallization and screening by electron microscopy. *Methods.* 41:417–426.

7. Engel, A., A. Hoenger, …, M. Zulauf. 1992. Assembly of 2-D membrane protein crystals: dynamics, crystal order, and fidelity of structure analysis by electron microscopy. *J. Struct. Biol.* 109:219–234.
8. Jap, B. K., M. Zulauf, …, A. Engel. 1992. 2D crystallization: from art to science. *Ultramicroscopy.* 46:45–84.
9. Kühlbrandt, W. 1992. Two-dimensional crystallization of membrane proteins. *Q. Rev. Biophys.* 25:1–49.
10. Mosser, G. 2001. Two-dimensional crystallogenesis of transmembrane proteins. *Micron.* 32:517–540.
11. Abeyrathne, P. D., M. Chami, …, H. Stahlberg. 2010. Preparation of 2D crystals of membrane proteins for high-resolution electron crystallography data collection. *Methods Enzymol.* 481:25–43.
12. Schmidt-Krey, I., W. Haase, …, W. Kühlbrandt. 2007. Two-dimensional crystallization of human vitamin K-dependent gamma-glutamyl carboxylase. *J. Struct. Biol.* 157:437–442.
13. Stuart, M. C., R. I. Koning, …, A. Brisson. 2004. Mechanism of formation of multilayered 2D crystals of the enzyme IIC-mannitol transporter. *Biochim. Biophys. Acta.* 1663:108–116.
14. Bichet, D., F. A. Haass, and L. Y. Jan. 2003. Merging functional studies with structures of inward-rectifier K(+) channels. *Nat. Rev. Neurosci.* 4:957–967.
15. Ashcroft, F. M. 2006. From molecule to malady. *Nature.* 440:440–447.
16. Clarke, O. B., A. T. Caputo, …, J. M. Gulbis. 2010. Domain reorientation and rotation of an intracellular assembly regulate conduction in Kir potassium channels. *Cell.* 141:1018–1029.
17. Kuo, A., J. M. Gulbis, …, D. A. Doyle. 2003. Crystal structure of the potassium channel KirBac1.1 in the closed state. *Science.* 300:1922–1926.
18. Nishida, M., M. Cadene, …, R. MacKinnon. 2007. Crystal structure of a Kir3.1-prokaryotic Kir channel chimera. *EMBO J.* 26:4005–4015.
19. Whorton, M. R., and R. MacKinnon. 2011. Crystal structure of the mammalian GIRK2 K+ channel and gating regulation by G proteins, PIP2, and sodium. *Cell.* 147:199–208.
20. Bavro, V. N., R. De Zorzi, …, S. J. Tucker. 2012. Structure of a KirBac potassium channel with an open bundle crossing indicates a mechanism of channel gating. *Nat. Struct. Mol. Biol.* 19:158–163.
21. Kuo, A., C. Domene, …, C. Vénien-Bryan. 2005. Two different conformational states of the KirBac3.1 potassium channel revealed by electron crystallography. *Structure.* 13:1463–1472.
22. Jarosławski, S., B. Zadek, …, S. Scheuring. 2007. Direct visualization of KirBac3.1 potassium channel gating by atomic force microscopy. *J. Mol. Biol.* 374:500–505.
23. Gupta, S., V. N. Bavro, …, M. R. Chance. 2010. Conformational changes during the gating of a potassium channel revealed by structural mass spectrometry. *Structure.* 18:839–846.
24. Domene, C., D. A. Doyle, and C. Vénien-Bryan. 2005. Modeling of an ion channel in its open conformation. *Biophys. J.* 89:L01–L03.
25. Paynter, J. J., I. Andres-Enguix, …, S. J. Tucker. 2010. Functional complementation and genetic deletion studies of KirBac channels: activatory mutations highlight gating-sensitive domains. *J. Biol. Chem.* 285:40754–40761.
26. Iacovache, I., M. Biasini, …, H. W. Rémigy. 2010. The 2DX robot: a membrane protein 2D crystallization Swiss Army knife. *J. Struct. Biol.* 169:370–378.
27. Kaufmann, T. C., A. Engel, and H. W. Rémigy. 2006. A novel method for detergent concentration determination. *Biophys. J.* 90:310–317.
28. Wang, H., and K. H. Downing. 2011. Specimen preparation for electron diffraction of thin crystals. *Micron.* 42:132–140.
29. Crowther, R. A., R. Henderson, and J. M. Smith. 1996. MRC image processing programs. *J. Struct. Biol.* 116:9–16.
30. Gipson, B., X. Zeng, and H. Stahlberg. 2007. 2dx_merge: data management and merging for 2D crystal images. *J. Struct. Biol.* 160:375–384.
31. Gipson, B., X. Zeng, …, H. Stahlberg. 2007. 2dx—user-friendly image processing for 2D crystals. *J. Struct. Biol.* 157:64–72.
32. Rigaud, J., M. Chami, …, J. Ranck. 2000. Use of detergents in two-dimensional crystallization of membrane proteins. *Biochim. Biophys. Acta.* 1508:112–128.
33. Zhao, G., M. C. Johnson, …, I. Schmidt-Krey. 2010. Two-dimensional crystallization conditions of human leukotriene C4 synthase requiring adjustment of a particularly large combination of specific parameters. *J. Struct. Biol.* 169:450–454.
34. Schenk, A. D., R. K. Hite, …, T. Walz. 2010. Electron crystallography and aquaporins. *Methods Enzymol.* 483:91–119.
35. Rigaud, J. L., B. Pitard, and D. Levy. 1995. Reconstitution of membrane proteins into liposomes: application to energy-transducing membrane proteins. *Biochim. Biophys. Acta.* 1231:223–246.
36. Dolder, M., A. Engel, and M. Zulauf. 1996. The micelle to vesicle transition of lipids and detergents in the presence of a membrane protein: towards a rationale for 2D crystallization. *FEBS Lett.* 382:203–208.
37. Michel, H., D. Oesterhelt, and R. Henderson. 1980. Orthorhombic two-dimensional crystal form of purple membrane. *Proc. Natl. Acad. Sci. USA.* 77:338–342.
38. Sonntag, Y., M. Musgaard, …, L. Thøgersen. 2011. Mutual adaptation of a membrane protein and its lipid bilayer during conformational changes. *Nat. Commun.* 2:1–7.
39. Collaborative Computational Project, Number 4. 1994. The CCP4 suite: programs for protein crystallography. *Acta Crystallogr. D Biol. Crystallogr.* 50:760–763.